Stable π-Extended Thio[7]helicene-based Diradical with Predominant Through-Space Spin-Spin Coupling

Hao Wu[1], Hiroki Hanayama[3], Max Coehlo[4], Yanwei Gu[1,9], Ze-Hua Wu[1], Satoshi Takebayashi[5], Gerhard Jakob[6], Serhii Vasylevskyi[7], Dieter Schollmeyer[8], Mathias Kläui[6], Grégory Pieters[4], Martin Baumgarten[1], Klaus Müllen[1,8,*], Akimitsu Narita[1,3,*] , Zijie Qiu[1,2,*]

[1] Max Planck Institute for Polymer Research, Ackermannweg 10, 55128 Mainz, Germany

[2] School of Science and Engineering, Shenzhen Institute of Aggregate Science and Technology, The Chinese University of Hong Kong, Shenzhen (CUHK-Shenzhen), Guangdong 518172, China

[3] Organic and Carbon Nanomaterials Unit, Okinawa Institute of Science and Technology Graduate University, 1919-1 Tancha, Onna-son, Kunigami-gun, Okinawa 904-0495, Japan

[4] Université Paris-Saclay, CEA, INRAE, Département Médicaments et Technologies pour la Santé (DMTS), SCBM, F-91191 Gif-sur-Yvette, France

[5] Science and Technology Group, Okinawa Institute of Science and Technology Graduate University, 1919-1 Tancha, Onna-son, Kunigami-gun, Okinawa 904-0495, Japan

[6] Institute of Physics, Johannes Gutenberg University Mainz, Staudinger Weg 7, 55128 Mainz, Germany

[7] Engineering Section, Research Support Division, Okinawa Institute of Science and Technology Graduate University, 1919-1 Tancha, Onna-son, Kunigami-gun, Okinawa 904-0495, Japan

[8] Department of Chemistry, Johannes Gutenberg University Mainz, Duesbergweg 10-14, 55128 Mainz, Germany

[9] Ningbo Institute of Materials Technology & Engineering, Chinese Academy of Sciences, Ningbo, Zhejiang, 315201 P. R. China

ABSTRACT: In this work, a novel π-extended thio[7]helicene scaffold was synthesized where the α-position of the thiophene unit could be functionalized with bulky phenoxy radicals after considerable synthetic attempts. This open-shell helical diradical, **ET7H-R**, possesses high stability in the air, non-trivial π conjugation, persistent chirality, and a high diradical character (y_0 of 0.998). The key feature is a predominant through-space spin-spin coupling (TSC) between two radicals in the helical terminals. Variable-temperature continuous-wave electron spin resonance (cw-ESR) and superconducting quantum interference device (SQUID) magnetometry in the solid state reveal a singlet ground state with a nearly degenerate triplet state of **ET7H-R**. These results highlight the significance of a stable helical diradicaloid as a promising platform for investigating intramolecular TSCs.

INTRODUCTION

[n]Helicenes, where *n* defines the number of aromatic rings, are *ortho*-fused polycyclic aromatic hydrocarbons (PAHs).[1-4] Their π-extended derivatives have drawn intensive attention in recent years owing to intrinsic chiral optoelectronic properties as well as high promise for asymmetric catalysis and chiral recognition.[5-12] When unpaired electrons are incorporated into helicenes, the merger of helical chirality and open-shell character can furnish magnetic materials with electrical magnetochiral anisotropy and chirality-induced spin selectivity (CISS).[13-16] Anion radicals of [6]helicene, formed by electron transfer reactions, are the pioneering examples whose studies, however, have been severely limited by the inherent high reactivity.[17] A few non-ionic open-shell helicenes have been achieved in recent years. Juríček *et al.* and Dumele *et al.* reported chiral diradicaloid photoswitches based on dimethylcethrene and dimethyl-[5]helicene, respectively.[18-19] Chueh, Chou, and Wu *et al.* developed a [7]helicene-based diradicaloid (Figure 1A) which exhibited a diradical character (y_0 = 0.23) and a triplet–singlet energy gap of 4.75 kcal/mol.[20] The Stępień group developed synthetic methods for a series of open-shell helicenes with different topologies and varied electronic characteristics (Figure 1B).[21]

The diradical characters in previously reported helical diradicaloids are relatively small, and the diradicaloid photoswitches give rise to closed-shell species. Moreover, the spins are mostly delocalized into the PAH backbone and thus coupled through π-conjugations similar to their planar counterparts. By contrast, the possible intramolecular through-space spin-spin coupling (TSC) via the spatial overlap of the helix has rarely been investigated. TSC, which largely depends on the distance between the two radical centers, has been utilized to determine the solution conformations of peptides, proteins, and polymers by electron spin resonance (ESR) technique.[22-24] It also plays a decisive role in determining the spin state of diradicals and triradicals.[25-26] For instance, a triplet ground state was established in cyclophane-based diradicals through TSC (Figure 1C).[27] Examples of diradicaloids with predominant diradical character, strong TSC, and stable chirality configuration are still rare which is mainly due to the limited availability of suitable scaffolds.

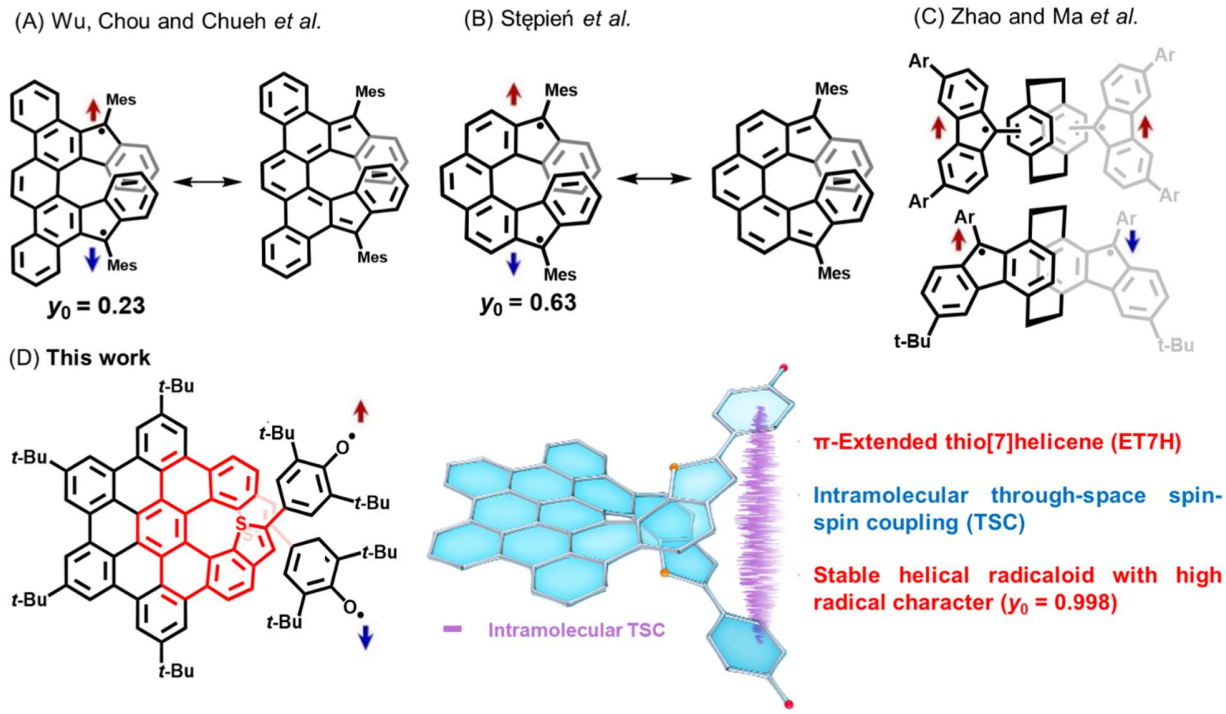

Figure 1. (A-B) [7]Helicene-based diradicaloids with y_0 = 0.23 and y_0 = 0.63. (C) A representative scaffold with the intramolecular through-space spin-spin coupling (TSC). (D) Left: molecular structure of π-extended thio[7]helicene-based stable phenoxy diradical. Right: schematic illustration of the intramolecular through-space coupling (purple).

In this work, a novel π-extended thio[7]helicene scaffold is synthesized incorporating two stable phenoxy radicals[28] in the helixes (Figure 1D). While density functional theory (DFT) calculations suggest a very high diradical character y_0 of 0.998, the targeted helical diradical **ET7H-R** is stable under air and thus allows structure characterization by single crystal analysis. Notably, a continuous-wave electron spin resonance (cw-ESR) spectrum at 100 K displays a zero-field splitting (ZFS), pointing toward an average distance of 9.49 Å between spins. The good agreement of this result with the distance between two phenoxy rings (9.84 Å) of **ET7H-R** from the single-crystal analysis reveals a dominant TSC in its helical NG structure with large π-conjugation. Measurements by a superconducting quantum-interference device (SQUID) indicate a singlet ground state with a thermally excited triplet state of **ET7H-R**. Further, a very small singlet-triplet gap (ΔE_{S-T}) is determined to be –0.07 kcal/mol, being consistent with variable-temperature cw-ESR results.

RESULTS AND DISCUSSION

The synthetic route to **ET7H-R** was explored as displayed in Schemes 1 and S1. 7-Bromobenzo[*b*]thiophene (**2**) was prepared through nucleophilic substitution and Friedel–Crafts ring-closure of compound **1** according to a literature procedure,[29] followed by a Stille coupling with bis(tributylstannyl)acetylene to furnish 1,2-bis(benzo[*b*]thiophen-7-yl)acetylene (**3**). Regioselective bromination of **3** at the α-positions of the thiophene units was achieved via lithiation with *n*-BuLi to yield 1,2-bis(2-bromobenzo[*b*]thiophen-7-yl)acetylene (**4**). Diarylacetylene **4** was then subjected to a Diels-Alder reaction with *tert*-butyl-substituted tetraphenylcyclopentadienone **5**[30] at 250 °C to obtain the precursor **6** in a modest yield of 56%. The cyclodehydrogenation of precursor **6** proceeded smoothly by using $FeCl_3$ as the oxidant and Lewis acid at room temperature, providing the π-extended dibromothio[7]helicene **S1** (Scheme S1).

For the introduction of the phenoxy radical units, we initially attempted the Suzuki coupling of **S1** and 3,5-di-*tert*-butyl-4-methoxyphenylboronic acid (**7**),[31] but the reaction failed with a variety of phosphine ligands which was apparently due to the large steric hindrance involved (Scheme S1). Alternatively, dibromide **6** was subjected to Suzuki coupling with boronic acid **7**, successfully providing precursor **8** in 85% yield (Scheme 1). After the Scholl reaction of **8** with $FeCl_3$, the formation of a dichlorinated product was indicated by mass spectrometry (Figure S1). Nonetheless, a dechlorination reaction could be accomplished using allyl-[1,3-bis-(2,6-diisopropylphenyl)-imidazol-2-yliden]-chloropalladium (CX21) and *t*-BuONa[32] to provide pure product **9** in 65% yield over two steps (Scheme 1).

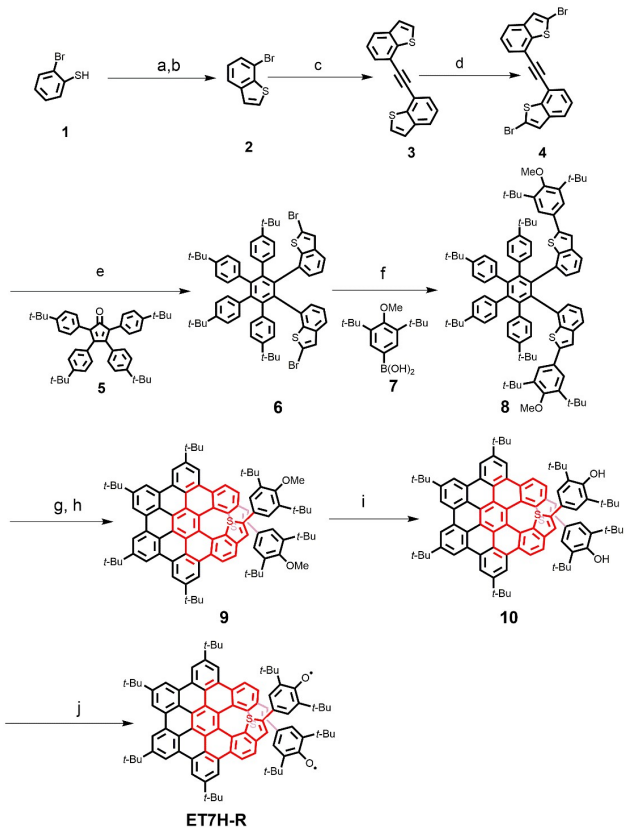

Scheme 1. Synthetic route toward **ET7H-R**. Reaction conditions: a) K_2CO_3, bromoacetaldehyde diethyl acetal, DMF, r.t.; b) polyphosphoric acid, chlorobenzene, reflux, 4 h, 90% yield in two steps; c) $Ph(PPh_3)_4$, toluene, bis(tributylstannyl)acetylene, 100 °C, 24 h, 85% yield; d) (1) *n*-BuLi, THF, -78 °C, 1 h; (2) Br_2, r.t., 1 h, 70% yield; e) diphenyl ether, 250 °C, 3 days, 56% yield; f) $Pd(PPh_3)_4$, K_2CO_3, dioxane/H_2O, 100 °C, overnight, 85% yield; g) $FeCl_3$, nitromethane, dichloromethane, r.t., 1 h; h) CX21, *t*-BuONa, THF/*i*-PrOH, 80 °C, overnight, 65% yield in two steps; i) ethanethiol, NaH, DMF, 0 °C, 0.5 h; then 100 °C, 12 h, 90% yield; j) PdO_2, CH_2Cl_2, r.t., 5 h.

Compound **9** has been fully characterized by NMR and single-crystal X-ray analysis (*vide infra*). For the demethylation of **9**, the use of BBr_3/Et_2O resulted in no reaction, but a condition with ethanethiol and NaH successfully afforded precursor **10** in 90% yield. DFT calculations were performed to identify the transition state. The isomerization barrier of **10** was calculated to be 52.6 kcal/mol (Figure S10A), indicating a high thermal stability of enantiomers of **10**. Chiral separation was achieved by high-performance liquid chromatography (HPLC) using a Daicel Chiralpak IE column. The chiroptical properties of **10** could thus be investigated using circular dichroism (CD) and circularly polarized luminescence (CPL) spectroscopies showing moderate absorption dissymmetry factor (g_{abs}) of 2.8×10^{-3} at 459 nm and luminescent dissymmetry factor (g_{lum}) of 2.7×10^{-3} (Figures S2-S3).

The generation of **ET7H-R** was initially attempted by treatment of precursor **10** with KOH and $K_3Fe(CN)_6$, whereby the presence of a large amount of monoradical impurity along with the diradical product was indicated by ESR spectroscopy (Figure S5). Nevertheless, the generation of **ET7H-R** was significantly improved by using PdO_2 as the oxidant, as revealed by the ESR analysis (*vide infra*). **ET7H-R** could be dissolved in common organic solvents such as dichloromethane, toluene, chloroform, and tetrahydrofuran, enabling further spectroscopic characterizations.

Compared to precursor **10**, the absorption bands of **ET7H-R** extended into the long wavelength region, showing the longest-wavelength peat at ~800 nm (Figure 2A).[33] The optical energy gap of **ET7H-R** was 1.44 eV based on the absorption onset of 860 nm. The stability of **ET7H-R** at ambient conditions was estimated by monitoring the radical-derived peak at 800 nm over time under air and room light (Figure 2B). After 20 hours, the intensity of the characteristic absorption band decreased to 87% of that in the freshly prepared solution (Figure 2C). When stored under a nitrogen atmosphere at 0 °C, **ET7H-R** was stable even over several weeks. Similar to precursor **10**, **ET7H-R** also possessed a high isomerization barrier of 51.0 kcal/mol by DFT calculations (Figure S10B). Accordingly, **ET7H-R** enantiomers could be enantiospecifically prepared from enantiomers of **10** without racemization under the mild oxidation condition (PdO_2, CH_2Cl_2, r.t., 5 h). CD spectra of **ET7H-R** enantiomers exhibited the Cotton effect in the long wavelength region (550-750 nm in Figure 2D) in agreement with the absorption spectrum (Figure 2A). Additionally, cyclic voltammetry (CV) measurements indicated a low reduction potential E_{red} of –0.53 eV for **ET7H-R** according to the onset of the reduction peak, in line with the formation of the radical anion from the diradical species (Figure S4).[34]

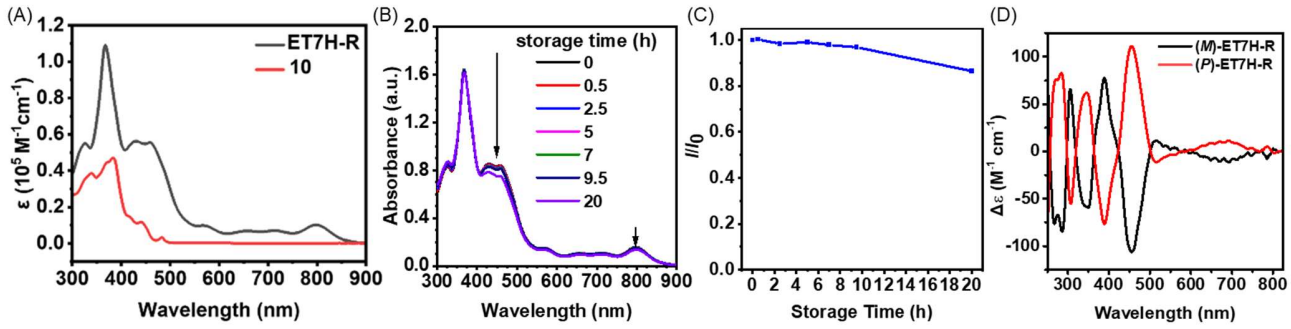

Figure 2. (A) UV-Vis-NIR absorption spectra of precursor **10** and **ET7H-R** in THF solution. Concentration: 10^{-5} M. (B-C) Stability analysis of **ET7H-R** in air monitored by absorption spectroscopy. I_0 is the absorbance of freshly prepared **ET7H-R** at 800 nm in THF

solution. *I* is the absorbance of the **ET7H-R** solution at 800 nm after storage in air for different numbers of hours. Concentration: 1.5×10^{-5} M. (D) CD spectra of **ET7H-R** measured in THF solution. Concentration: 10^{-5} M.

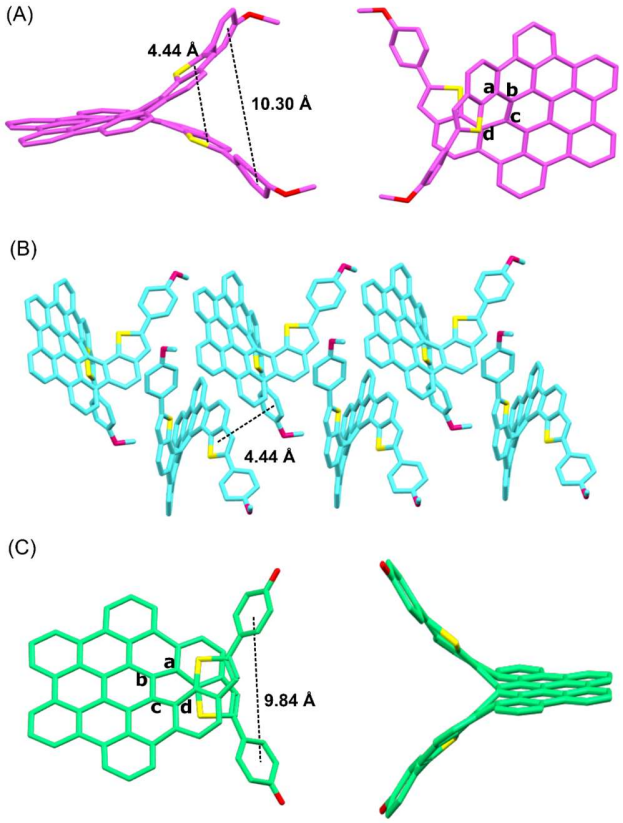

Figure 3. (A) Side-view and top-view of the single-crystal structure of compound **9**. (B) Molecular packing of compound **9**. All hydrogen atoms and the *tert*-butyl groups were omitted for clarity. (C) Side-view and top-view of the single-crystal structure of **ET7H-R**.

Single crystals of the dimethoxy derivative **9** (CCDC: 2239700) and the diradical species **ET7H-R** (CCDC: 2291841) suitable for X-ray diffraction analysis could be obtained by slow diffusion of methanol into a dichloromethane solution of **9**, as well as slow evaporation of a cyclohexane solution of **ET7H-R**, respectively. As depicted in Figures 3A and C, the helical structures of **9** and **ET7H-R** were unambiguously confirmed, although the final R1 value of the latter (= 11.53%) is relatively high due to the crystallographic disorder, especially overlapping of two enantiomers. Compound **9** possessed the torsion angle (atoms a−b−c−d) of 35° and the long helical pitch (4.44 Å) determined from the centroid−centroid distance of the overlapping thiophene rings. The sigma bond distance and the interplane angle between the methoxyphenyl and thiophene ring were measured as 1.47 Å in average (Table S5) and 31.9(6)° to 41.4(7)° (Table S6), respectively. The centroid−centroid distance of the two methoxyphenyl rings was 10.30 Å in **9**. Intriguingly, although a racemic mixture in solution was used to grow crystals, only one enantiomer was found in the single crystal of **9** via orthorhombic packing with moderate intermolecular π-π-interactions (Figure 3B).

Similar to **9**, the sigma bond distance between the phenoxy radical and the thiophene ring in **ET7H-R** were measured as 1.50(2) Å in average (Table S9) with the interplane angle of 6(4)° to 27(2)° (Table S11) in the crystal data. Additional DFT optimizations were performed to assist the conformational analyses of **ET7H-R**. The C-O lengths were 1.222(9) and 1.257(11) Å in the **ET7H-R** crystal (Figure 3C and Table S9) and 1.24 Å in the DFT-optimized conformation (Figure S9). Both of these values were shorter than the C-O single bond length (1.39 Å) in **9** (Table S5), supporting the successful diradical formation.[33] The centroid−centroid distance of the two phenoxy rings was found from DFT to be 10.25 Å, which was larger than 9.84 Å in the crystal data.

The highest occupied molecular orbital (HOMO) and lowest unoccupied molecular orbital (LUMO) of **ET7H-R** were calculated by DFT simulations (Figure S8). According to Clar's rule, the diradical resonance structure (**ET7H-R**) with seven Clar's sextets (marked in light blue) should be predominant over the quinoid counterpart (**ET7H-Q**) with only two Clar's sextets (Figure 4A). The diradical character y_0 of **ET7H-R** was calculated to be 0.998 by Yamaguchi's scheme,[35] suggesting its almost pure diradical nature in agreement with Clar's rule. Moreover, the calculation of the spin density distribution by DFT suggested the localization of spins mainly on the phenoxy groups with only a little delocalization into the π-conjugated polycyclic skeleton (Figure 4B). Therefore, the predominant TSC in **ET7H-R** can be ascribed to the Clar's rule in addition to the suitable spatial arrangement of two spins.

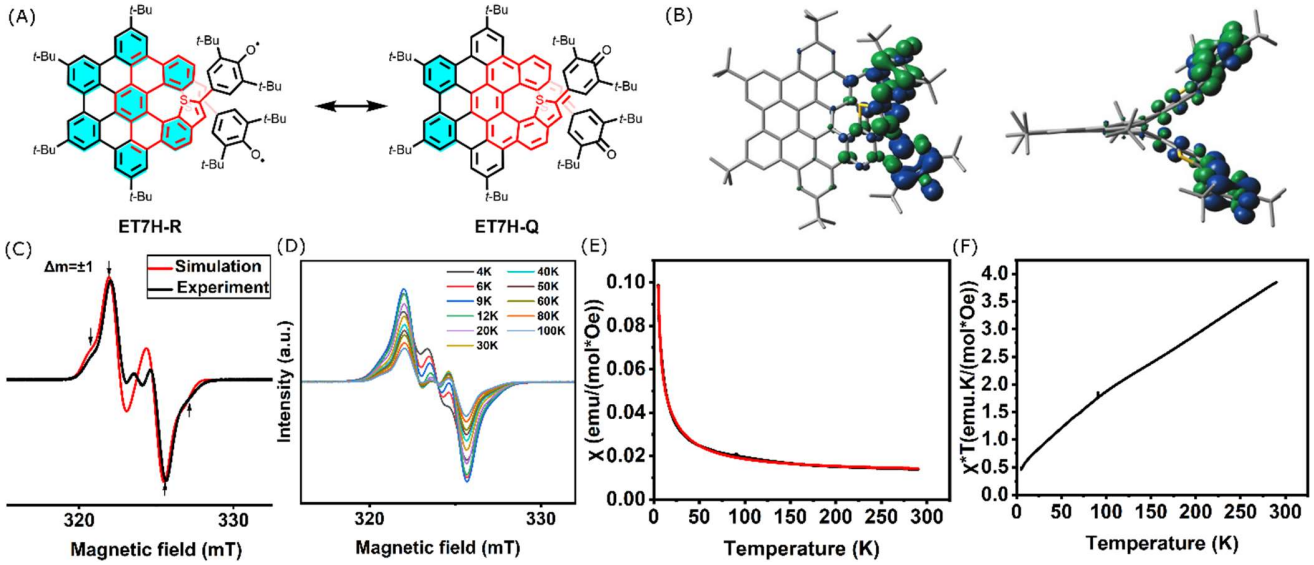

Figure 4. (A) Resonance of the radical form **ET7H-R** and quinoid structure **ET7H-Q**. Clar sextets are marked in light blue. (B) Top-view and side-view of spin-distribution of **ET7H-R** simulated by DFT (UB3LYP/6-311G(d,p). (C) Experimental and simulated X-band cw-ESR spectrum of **ET7H-R** at 100 K. The simulation was conducted with D = 32.5 G and E = 0 G). (D) Variable-temperature cw-ESR spectra of **ET7H-R** in the temperature range of 4-100 K in toluene. (E) SQUID measurements of **ET7H-R** in the temperature range of 5-290 K (black) and the curve fitted by the Bleaney-Bowers equation with the Curie-Weiss law and van Vleck susceptibility contributions (red). (F) The χ*T-T by SQUID measurements (measured in the fixed field of 0.1 T).

To further explore the intrinsic magnetic properties of **ET7H-R**, cw-ESR measurements were conducted. At room temperature, the cw-ESR spectrum of **ET7H-R** in dilute toluene solution (5×10^{-4} M) exhibited a complex hyperfine splitting due to multiple interactions with neighboring hydrogen atoms (Figure S6). When the cw-ESR of **ET7H-R** was measured in frozen toluene (100K), clear shoulder peaks associated with zero-field splitting (ZFS) (Δm_s =±1) were observed (Figure 4C). The prominent ZFS signal suggested a significant triplet population with strong spin-spin coupling. The ZFS parameters, D and E for axial and transversal components of the magnetic dipole–dipole interaction, were 32.5 G and 0 G, respectively.

Based on the point-dipole approximation, the D parameter is inversely proportional to the $\langle r \rangle^3$:

$$\langle r \rangle^3 = \left[\frac{5.56 \times 10^4}{|2D|}\right]$$

where $\langle r \rangle$ is the average distance between spins over all possible electronic positions.[36,37] Therefore, the average distance $\langle r \rangle$ was assessed as 9.49 Å, similar to the spatial centroid−centroid distance of two phenoxy rings from the single-crystal analysis of **ET7H-R** (9.84 Å in Figure 3C). This key result indicates that spin-spin coupling is mainly originating from the through-space interaction over the through-bond conjugation.

To address the ground state of **ET7H-R**, a variable-temperature ESR experiment was performed from 4 to 100 K in toluene (Figure 4D). The I*T vs T curve, where I is the ESR resonance intensity and T is the corresponding temperature, is plotted in Figure S7. An increasing paramagnetic signal was observed as elevating the temperature, which revealed a singlet ground state with a thermally excited triplet state. By fitting the I*T-T plot with a modified Bleaney-Bowers equation, assuming contributions from doublet impurities as constant,[27,38] the singlet-triplet gap ΔE_{S-T} was roughly estimated to be approximately -0.05 kcal/mol, qualitatively suggesting a singlet ground state with a nearly degenerate triplet state of **ET7H-R**. The magnetic susceptibility χ of **ET7H-R** was also investigated in the solid state by SQUID measurements from 5 to 290 K (Figure 4E). It is worth noting that the intermolecular spin-spin coupling also contributed to the SQUID results of the solid powder in additional to the intramolecular TSC. The magnetic molar susceptibility exhibited a continuous increase when decreasing the temperature and a good linear relationship between χ*T and T was found in Figure 4F. Fitted by the Bleaney-Bowers equation including the Curie-Weiss law and van Vleck susceptibility contributions,[27] the ΔE_{S-T} was -0.07 kcal/mol which was in line with the approximate value from the ESR analysis in the toluene solution (see the SI for details). Therefore, the magnetic properties determined by both SQUID and ESR experiments convincingly support the TSC in **ET7H-R**.

CONCLUSION

In summary, a stable π-extended thio[7]helicene-based diradical **ET7H-R** with a high diradical character (y_0 = 0.998) was synthesized. While maintaining a large conjugated system, a predominant intramolecular TSC was revealed by DFT calculations, cw-ESR spectra, SQUID measurement, and single-crystal analysis. From the synthesis point of view, the efficient functionalization at the

α-positions of thiophene units opens up numerous opportunities to incorporate different building blocks into this novel π-extended thio[7]helicene to utilize the spatial overlapping of the helical terminals. Consequently, this π-extended thio[7]helicene will serve as a promising scaffold to investigate delicate intramolecular through-space interactions for diverse chiral optoelectronic applications in the future.

ASSOCIATED CONTENT

Supporting Information

Experimental details, characterization spectra of all synthesized compounds, single-crystal data, photophysical measurements, and computational details. This material is available free of charge via the Internet at http://pubs.acs.org.

AUTHOR INFORMATION

Corresponding Authors

*muellen@mpip-mainz.mpg.de
*akimitsu.narita@oist.jp
*zijieqiu@cuhk.edu.cn

ORCID
Yanwei Gu: 0000-0003-1718-5868
Satoshi Takebayashi: 0000-0002-0647-3365
Gerhard Jakob: 0000-0001-9466-0840
Martin Baumgarten: 0000-0002-9564-4559
Grégory Pieters: 0000-0002-3924-8287
Klaus Müllen: 0000-0001-6630-8786
Akimitsu Narita: 0000-0002-3625-522X
Zijie Qiu: 0000-0003-0728-1178

Notes

The authors declare no competing financial interests.

ACKNOWLEDGMENT

This work is financially supported by the Max Planck Society, Shenzhen Key Laboratory of Functional Aggregate Materials (ZDSYS20211021111400001), the Science, Technology and Innovation Commission of Shenzhen Municipality (KQTD20210811090142053, JCYJ20220530143805012), the FLAG-ERA Grant OPERA by DFG 437130745, the ANR-DFG NLE Grant GRANAO by DFG 431450789, the Johannes Gutenberg-Universität Mainz (JGU) through a Gutenberg Research College Fellowship, the Okinawa Institute of Science and Technology Graduate University (OIST), and start-up funding at the Chinese University of Hong Kong, Shenzhen (UDF01002468). We appreciate the help and support provided by the Instrumental Analysis Section of the Research Support Division at OIST.

REFERENCES

(1) Dhbaibi, K.; Favereau, L.; Crassous, J. Enantioenriched Helicenes and Helicenoids Containing Main-Group Elements (B, Si, N, P). *Chem. Rev.* **2019**, *119* (14), 8846-8953.
(2) Gingras, M. One hundred years of helicene chemistry. Part 1: non-stereoselective syntheses of carbohelicenes. *Chem. Soc. Rev.* **2013**, *42* (3), 968-1006.
(3) Mori, K.; Murase, T.; Fujita, M. One-step synthesis of [16]helicene. *Angew. Chem., Int. Ed.* **2015**, *54* (23), 6847-6851.
(4) Shen, Y.; Chen, C. F. Helicenes: synthesis and applications. *Chem. Rev.* **2012**, *112* (3), 1463-1535.
(5) Ernst, K. H. Stereochemical Recognition of Helicenes on Metal Surfaces. *Acc Chem. Res.* **2016**, *49* (6), 1182-1190.
(6) Qiu, Z.; Ju, C. W.; Frederic, L.; Hu, Y.; Schollmeyer, D.; Pieters, G.; Mullen, K.; Narita, A. Amplification of Dissymmetry Factors in pi-Extended [7]- and [9]Helicenes. *J. Am. Chem. Soc.* **2021**, *143* (12), 4661-4667.
(7) Tanaka, H.; Inoue, Y.; Mori, T. Circularly Polarized Luminescence and Circular Dichroisms in Small Organic Molecules: Correlation between Excitation and Emission Dissymmetry Factors. *ChemPhotoChem* **2018**, *2* (5), 386-402.
(8) Teichmann, B.; Krause, A. M.; Lin, M. J.; Wurthner, F. Enantioselective Recognition of Helicenes by a Tailored Chiral Benzo[ghi]perylene Trisimide pi-Scaffold. *Angew. Chem., Int. Ed.* **2022**, *61* (15), e202117625.
(9) Wu, Y. F.; Ying, S. W.; Su, L. Y.; Du, J. J.; Zhang, L.; Chen, B. W.; Tian, H. R.; Xu, H.; Zhang, M. L.; Yan, X.; et al. Nitrogen-Embedded Quintuple [7]Helicene: A Helicene-Azacorannulene Hybrid with Strong Near-Infrared Fluorescence. *J. Am. Chem. Soc.* **2022**, *144* (24), 10736-10742.
(10) Xiao, X.; Pedersen, S. K.; Aranda, D.; Yang, J.; Wiscons, R. A.; Pittelkow, M.; Steigerwald, M. L.; Santoro, F.; Schuster, N. J.; Nuckolls, C. Chirality Amplified: Long, Discrete Helicene Nanoribbons. *J. Am. Chem. Soc.* **2021**, *143* (2), 983-991.
(11) Izquierdo-Garcia, P., Fernandez-Garcia, J. M.; Medina Rivero, S.; Samal, M.; Rybacek, J.; Bednarova, L.; Ramirez-Barroso, S.; Ramirez, F. J.; Rodriguez, R.; Perles, J.; et al. Helical Bilayer Nanographenes: Impact of the Helicene Length on the Structural, Electrochemical, Photophysical, and Chiroptical Properties. *J. Am. Chem. Soc.* **2023**, *145* (21), 11599-11610.
(12) Takenaka N., Chen J., Captain B., Sarangthem R., Chandrakumar A. Helical Chiral 2-Aminopyridinium Ions: A New Class of Hydrogen Bond Donor Catalysts. *J. Am. Chem. Soc.* **2010**, *132*, 4536–4537.
(13) Krstić, V.; Roth, S.; Burghard, M.; Kern, K.; Rikken, G. L. J. A. Magneto-chiral anisotropy in charge transport through single-walled carbon nanotubes *J. Chem. Phys.* **2022**, *117*, 11315–11319
(14) Pop, F.; Auban-Senzier, P.; Canadell, E.; Rikken, G. L.; Avarvari, N. Electrical magnetochiral anisotropy in a bulk chiral molecular conductor. *Nat. Commun.* **2014**, *5*, 3757.
(15) Göhler, B.; Hamelbeck, V.; Markus, T. Z.; Kettner, M.; Vager, G. F. H. Z.; Naaman, R.; Zacharias, H. Spin Selectivity in Electron Transmission Through Self-Assembled Monolayers of Double-Stranded DNA. *Science* **2011**, *331*, 894-896.
(16) Kiran, V.; Mathew, S. P.; Cohen, S. R.; Hernandez Delgado, I.; Lacour, J.; Naaman, R. Helicenes--A New Class of Organic Spin Filter. *Adv. Mater.* **2016**, *28* (10), 1957-1962.
(17) Allendoerfer, R. D.; Chang, R. An ESR and ENDOR Study of the Hexahelicene Anion Radical. *J. Magn. Reson.* **1971**, *5* (2), 273-277.
(18) Ravat, P.; Solomek, T.; Haussinger, D.; Blacque, O.; Juricek, M. Dimethylcethrene: A Chiroptical Diradicaloid Photoswitch. *J. Am. Chem. Soc.* **2018** 140 (34), 10839-10847.
(19) Gunther, K.; Grabicki, N.; Battistella, B.; Grubert, L.; Dumele, O. An All-Organic Photochemical Magnetic Switch with Bistable Spin States. *J. Am. Chem. Soc.* **2022**,144(19), 8707-8716.
(20) Hsieh, Y.- C.; Wu, C.-F.; Chen, Y.-T.; Fang, C.-T.; Wang, C.-S.; Li, C.-H.; Chen, L.-Y.; Cheng, M.-J.; Chueh, C.-C.; Chou, P.-T.; Wu, Y.-T. 5,14-Diaryldiindeno[2,1- f:1',2' -j]picene: A New Stable [7]Helicene with a Partial Biradical Character. *J. Am. Chem. Soc.* **2018**, 140(43), 14357-14366.
(21) Borissov, A.; Chmielewski, P. J.; Gomez Garcia, C. J.; Lis, T.; Stepien, M. Dinor[7]helicene and Beyond: Divergent Synthesis of Chiral Diradicaloids with Variable Open-Shell Character. *Angew. Chem., Int. Ed.* **2023**, *62* (38), e202309238.
(22) Miick, S. M.; Martinez, G. V.; Fiori, W. R.; Todd, A. P.; Millhauser, G. L. Short alanine-based peptides may form 3_{10}-

helices and not α-helices in aqueous solution. *Nature* **1992**, *359*, 653-655.
(23) Matsuda, K.; Stone, M. T.; Moore, J. S. Helical Pitch of m-Phenylene Ethynylene Foldamers by Double Spin Labeling. *J. Am. Chem. Soc.* **2002**, *124*, 11836-11837.
(24) Bosman, A. W.; Janssen, R. A. J.; Meijer, E. W. Five Generations of Nitroxyl-Functionalized Dendrimers. *Macromolecules* **1997**, *30* (12), 3606-3611.
(25) Kodama, T.; Aoba, M.; Hirao, Y.; Rivero, S. M.; Casado, J.; Kubo, T. Molecular and Spin Structures of a Through-Space Conjugated Triradical System. *Angew. Chem., Int. Ed.* **2022,** 61(14), e202200688.
(26) Kodama, T.; Hirao, Y., Kubo, T. Synthesis and Properties of a Through-Space Interacting Diradicaloid. *Precis. Chem.* **2023,** 1(3), 183-191.
(27) Han, H.; Zhang, D.; Zhu, Z.; Wei, R.; Xiao, X.; Wang, X.; Liu, Y.; Ma, Y.; Zhao, D. Aromatic Stacking Mediated Spin-Spin Coupling in Cyclophane-Assembled Diradicals. *J. Am. Chem. Soc.* **2021**, 143 (42), 17690-17700.
(28) Canesi E. V.; Fazzi, D.; Colella, L.; Bertarelli, C.; Castiglioni, C. Tuning the Quinoid versus Biradicaloid Character of Thiophene-Based Heteroquaterphenoquinones by Means of Functional Groups. *J. Am. Chem. Soc.* **2012,** 134, (46), 19070-19083.
(29) Hansen, M.; Jacobsen, S. E.; Plunkett, S.; Liebscher, G. E.; McCorvy, J. D.; Brauner-Osborne, H.; Kristensen, J. L. Synthesis and pharmacological evaluation of N-benzyl substituted 4-bromo-2,5-dimethoxyphenethylamines as 5-HT2A/2C partial agonists. *Bioorg. Med. Chem*. **2015,** 23(14), 3933–3937.
(30) Lungerich D., Hitzenberger J. F., Marcia M., Hampel F., Drewello T., Jux N. Superbenzene–Porphyrin Conjugates. *Angew. Chem., Int. Ed.* **2014,** 53(45), 12231 –12235.
(31) Rathnayake, H. P, Cirpan, A., Delen, Z., Lahti, P. M, Karasz, F. E. Optimizing OLED Efficacy of 2,7-Diconjugated 9,9-Dialkylfluorenes by Variation of Periphery Substitution and Conjugation Length. *Adv. Funct. Mater,* **2007,** 17(1), 115-12.
(32) Navarro O., Kaur H., Mahjoor P., Nolan S. Cross-Coupling and Dehalogenation Reactions Catalyzed by (N-Heterocyclic carbene)Pd(allyl)Cl Complexes, *J. Org. Chem.,* **2004,** 69 (9), 3173–3180.
(33) Morita Y.; Ueda A.; Nishida S.; Fukui K.; Ise T.; Shiomi D.; Sato K.; Takui T.; Nakasuji K. Curved Aromaticity of a Corannulene-Based Neutral Radical: Crystal Structure and 3D Unbalanced Delocalization of Spin. *Angew. Chem. Int .Ed.* **2008**, 47 (11), 2035–2038.
(34) Intorp, S. N.; Hodecker, M.; Muller, M.; Tverskoy, O.; Rosenkranz, M.; Dmitrieva, E.; Popov, A. A.; Rominger, F.; Freudenberg, J.; Dreuw, A.; et al. Quinoidal Azaacenes: 99 % Diradical Character. *Angew. Chem., Int. Ed.* **2020,** 59 (30), 12396-12401.
(35) Yamaguchi, K. *Chem. Phys. Lett.* **1975,** 33, 330.
(36) Gleason, W. B.; Barnett, R. E. Use of the Point Dipole Approximation for Nitroxide Biradicals. *J. Am. Chem. Soc.* **1976,** 98 (10), 2701-2705.
(37) Zoppellaro, G.; Geies, A.; Enkelmann, V.; Baumgarten, M.. 2,6-Bis(pyrazolyl)pyridine Functionalised with Two Nitronylnitroxide and Iminonitroxide Radicals. *Eur. J. Org. Chem.* **2004**, 2367-2374.
(38) Bleaney, B.; Bowers, K. D. Anomalous paramagnetism of copper acetate. *Proc. R. Soc. London, Ser. A* **1952,** 214 (214), 451-465.

Table of Contents

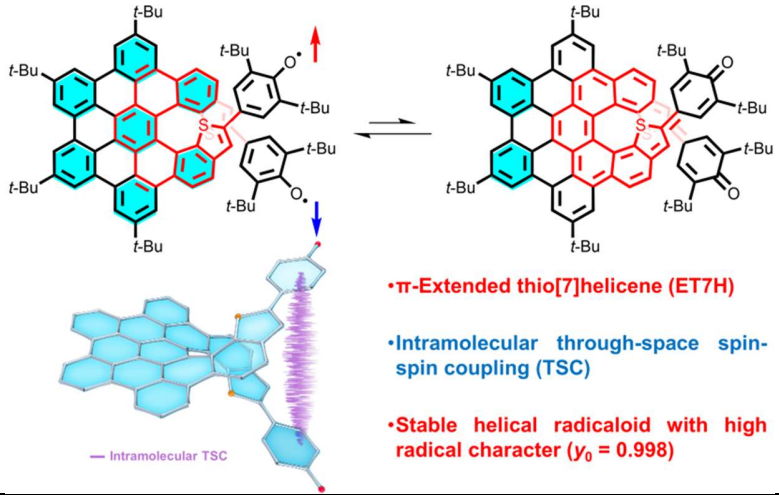

•π-Extended thio[7]helicene (ET7H)

•Intramolecular through-space spin-spin coupling (TSC)

•Stable helical radicaloid with high radical character (y_0 = 0.998)